

# Coherent Photoproduction of Pions on Nuclei in a relativistic, non-local Model \* †

W. Peters<sup>‡</sup>, H. Lenske and U. Mosel

*Institut für Theoretische Physik, Universität Giessen  
D-35392 Giessen, Germany*

## Abstract

A relativistic and non-local model for the coherent photoproduction of pions on nuclei is presented. The production operator is derived from an effective Lagrangian model that contains all the degrees of freedom known to contribute to the elementary process. Using the framework of DWIA, the matrix elements of this operator are evaluated using relativistic bound state wave functions. Final state interactions are accounted for via a pion-nucleus optical potential. The effects of in-medium modifications of the production operator are discussed. We give results for  $^{12}\text{C}$  and  $^{40}\text{Ca}$ , and compare our calculations to the data of the A2 collaboration at MAMI.

## I. INTRODUCTION

Photonuclear reactions offer a unique possibility to test our understanding of hadrons in vacuum as well as within a nuclear environment. For elementary reactions like the photoproduction of pions, relativistic models based on an effective Lagrangian approach are well established by now (see for example [1] and references therein). Starting from the elementary process, numerous studies treat the photoproduction of pions on nuclei. Among the large number of possible reactions, the coherent photoproduction plays a special role. Since in this case the nucleus remains in the ground state after the reaction process, the amount of further theoretical assumptions is smaller than e.g. in the case of reactions like  $(\gamma, \pi N)$  or completely inclusive processes like photoabsorption on nuclei. In this sense the coherent photoproduction of pions is the cleanest test for any model that treats photoproduction of pions on nuclei.

---

\*Work supported by BMBF and GSI Darmstadt.

†This work forms part of the dissertation of W. Peters.

‡Wolfram.Peters@theo.physik.uni-giessen.de

The first data on coherent photoproduction of pions on nuclei were given in [2]. The extraction of the coherent events in this experiment, however, was uncertain, so that comparison to these data is not very conclusive. In [3], the differential cross section was given for a photon energy of  $E_\gamma \approx 175$  MeV. It is, however, a special feature of the coherent process, that the differential cross section is mainly sensitive to the nuclear form factor (see Sec. II C). Since the nuclear wave functions, and therefore the bound state properties of the nucleus are taken as an input, all models yield more or less the correct shape of the differential cross section as can be seen in [3]. For a given energy they differ mainly with respect to the absolute value of the cross section. To further distinguish between different models, energy dependent data are needed. Thus the new data of the A2-collaboration at MAMI [4], which give the differential cross section at a fixed angle for a large energy range between 140 MeV and 430 MeV, are highly welcome. They enable us to test our calculations not only close to threshold, but over the entire  $\Delta$  region.

Part of the existing calculations for the coherent photoproduction of pions work in the delta-hole model ([5–7] and references therein). These calculations treat the  $\Delta$  and pion dynamics in a very sophisticated manner, however, non-resonant contributions can only be estimated [7]. Another group of models use the distorted wave impulse approximation (DWIA) [8–11]. These studies take into account the non-resonant contributions, but resort for technical reasons to non-relativistic and local approximations.

In contrast to these studies, we present a relativistic and non-local calculation in the framework of DWIA. Since the commonly used approximations are not made, this approach reduces the theoretical uncertainties greatly, but requires a larger technical effort.

In the following section we first describe the elementary production operator we use. After some general remarks on the coherent photoproduction of pions, we then give the details of our model. Results for PWIA, as well as DWIA calculations are shown in Sec. III. We finally discuss the effects of in-medium modifications of the production operator. In Sec. IV the results of our study are summarized.

## II. THE MODEL

### A. The elementary operator

The diagrams contributing to the elementary process of photoproduction of neutral pions on a single nucleon are shown in Fig. 1: There are the direct and crossed nucleon graph, the direct and crossed  $\Delta$ -graph and the graph containing the omega meson in the  $t$ -channel. There could in principle also be an analogous graph containing the rho meson, but due the smallness of the corresponding couplings it contributes only negligibly to the production of neutral pions [1]. We use the following interaction terms:

$$\begin{aligned}\mathcal{L}_{\pi NN} &= -\frac{g_{\pi NN}}{m_\pi} \bar{\psi} \gamma_5 (\not{\partial} \vec{\pi}) \vec{\tau} \psi \\ \mathcal{L}_{\gamma NN} &= -e \bar{\psi} \frac{1}{2} (1 + \tau_3) \gamma_\mu \psi A^\mu \\ &\quad -\frac{1}{2} e \frac{\kappa_p}{2m_N} \bar{\psi} \frac{1}{2} (1 + \tau_3) \sigma_{\mu\nu} \psi F^{\mu\nu}\end{aligned}$$

$$\begin{aligned}
& -\frac{1}{2} e \frac{\kappa_n}{2m_N} \bar{\psi} \frac{1}{2}(1 - \tau_3) \sigma_{\mu\nu} \psi F^{\mu\nu} \\
\mathcal{L}_{\pi N\Delta} &= \frac{g_{\pi N\Delta}}{m_\pi} \bar{\psi}_\Delta^\mu (\partial_\mu \vec{\pi}) \vec{T} \psi + \text{h.c.} \\
\mathcal{L}_{\gamma N\Delta} &= \frac{ie g_{\gamma N\Delta}}{m_\pi} \bar{\psi}_\Delta^\mu \gamma^\nu \gamma_5 T_3 \psi F_{\mu\nu} + \text{h.c.} \\
\mathcal{L}_{\omega\pi\gamma} &= \frac{eg_{\omega\pi\gamma}}{4m_\pi} \varepsilon_{\mu\nu\rho\sigma} (V^{\mu\nu} F^{\rho\sigma}) \pi \\
\mathcal{L}_{\omega NN} &= -g_{\omega NN}^v \bar{\psi} \gamma_\mu \psi \omega^\mu \\
& \quad -\frac{1}{2} \frac{g_{\omega NN}^t}{2m_N} \bar{\psi} \sigma_{\mu\nu} \psi V^{\mu\nu} \quad , \tag{1}
\end{aligned}$$

with  $F_{\mu\nu} = \partial_\mu A_\nu - \partial_\nu A_\mu$  and  $V_{\mu\nu} = \partial_\mu \omega_\nu - \partial_\nu \omega_\mu$ , where  $A_\mu(\omega_\mu)$  denotes the photon (omega) field.

For the  $\Delta$ -propagator we take [12]:

$$G_\Delta^{\mu\nu}(p) = i \frac{\not{p} + m_\Delta}{s - m_\Delta^2 + i\sqrt{s} \Gamma(s)} \Lambda^{\mu\nu} \tag{2}$$

with

$$\Lambda^{\mu\nu} = \left( g^{\mu\nu} - \frac{1}{3} \gamma^\mu \gamma^\nu - \frac{2}{3m_\Delta^2} p^\mu p^\nu - \frac{1}{3m_\Delta} (\gamma^\mu p^\nu - p^\mu \gamma^\nu) \right) . \tag{3}$$

The width of the  $\Delta$  is taken to depend on the energy:

$$\Gamma(s) = \Gamma_o \frac{m_\Delta}{\sqrt{s}} \left( \frac{q}{q_o} \right)^3 \left( \frac{q_o^2 + c^2}{q^2 + c^2} \right)^2 \tag{4}$$

with  $\Gamma_o = 120$  MeV and  $c = 0.5$  GeV.  $q$  and  $q_o$  denote the momentum of the pion resulting from a decay of a  $\Delta$  of a mass  $\sqrt{s}$  and of 1.232 GeV, respectively, in the rest-frame of the  $\Delta$ .

For the coupling constants we use the following values:

$$\begin{aligned}
e &= 0.3028 \quad , \quad g_{\pi NN} = 0.97 \\
\kappa_p &= 1.79 \quad , \quad \kappa_n = -1.91 \\
g_{\pi N\Delta} &= 2.1 \quad , \quad g_{\gamma N\Delta} = 0.34 \\
g_{\omega\pi\gamma} &= 0.313 \quad , \quad g_{\omega NN}^v = 10 \\
g_{\omega NN}^t &= 1.4 \quad . \tag{5}
\end{aligned}$$

The coupling constants of the photon and the pion to the nucleon are well known. The value we use for  $g_{\pi N\Delta}$  corresponds to an on-shell decay width of the  $\Delta$  of 120 MeV, so that it is consistent with  $\Gamma_o$  in Eq. (4).  $g_{\omega\pi\gamma}$  has been determined from the decay width of an omega meson into a pion and a photon [1]. For the couplings of the omega to the nucleon different values are used in the literature; the values given in (5) are taken from [13]. The

contribution of the omega graph to the photoproduction of pions or eta mesons is small, so that the  $\omega NN$  coupling constants cannot be determined by fitting the experimental data for these processes [14,15]. Instead, they are taken from  $NN$  scattering [16], or they are derived from the  $\rho NN$  parameters via  $SU(3)$  considerations [17]. The values for  $g_{\omega NN}^v$  used in the literature for photoproduction processes range from 8 [17] to 17 [18]. In addition, a form factor is introduced at the  $\omega NN$ -vertex:

$$F(t) = \frac{\Lambda^2 - m_\omega^2}{\Lambda^2 - t} \quad , \quad (6)$$

with  $\Lambda^2 = 2 \text{ GeV}^2$  [14]. The sensitivity of our results to the omega parameters will be discussed in Sec. III.

Finally,  $g_{\gamma N\Delta}$  and  $c$  in Eq. (4) were adjusted such that the data for the cross section for the photoproduction of neutral pions on protons [19] are well reproduced (Fig. 2).

## B. Photoproduction on the nucleus

After having specified the elementary production operator we now turn to the photoproduction on the nucleus. The framework commonly used for exclusive processes like the coherent photoproduction is the DWIA. Here it is assumed that the production process involves only a single nucleon, while for the distortions of in- or outgoing particles interactions with the entire nucleus are taken into account. The single-particle production operator is taken from an elementary model and evaluated using realistic bound state and scattering state wave functions instead of plane waves. Since the nucleon participating in this reaction is bound in a potential, it is off-shell, and the production operator must be evaluated for kinematical situations different from the one in the free case.

For technical reasons a relativistic production operator is often simplified using on-shell relations or a non-relativistic reduction [18], in order to make its evaluation easier. The resulting production operators are more or less equivalent on-shell, but the off-shell behavior is not the same as for the original operator. To avoid this problem, we take the production operator in its original form from the model described in the previous section, without rewriting it. Thus we use the natural off-shell dependence resulting from an effective field theory.

A numerical complication arises from the fact that the production operator depends on the momentum of the incoming nucleon, i.e. it is non-local. To circumvent complicated integrations, most DWIA calculations evaluate the production operator at some fixed effective nucleon momentum. For knock-out processes like  $(\gamma, \pi N)$ , where the asymptotic momenta of the outgoing particles can be used to estimate the momentum arguments of the production operator, the validity of this approximation is discussed in [20]. In the case of coherent production, both the incoming and the outgoing nucleon are in a bound state, so that they do not have a well defined asymptotic momentum. To avoid the uncertainties related to the local approximation, we evaluate the matrix elements of the production operator completely non-locally. We will discuss the local and the non-relativistic approximation further in Sec. III.

### C. The coherent process

In the nuclear coherent photoproduction of pions, the nucleus remains in the ground state after the reaction. In the case of spin zero nuclei ( $A$ ) like  $^{12}\text{C}$  or  $^{40}\text{Ca}$  the quantum numbers of the participants are:

$$1_{\gamma}^{-} + 0_A^{+} \rightarrow 0_{\pi}^{-} + 0_A^{+} \quad . \quad (7)$$

Since the pion in the final state has the quantum numbers  $0^{-}$ , i.e. it has unnatural parity, the Lorentz invariant amplitude for the entire process must have the form [21]:

$$T^{(\lambda)} = \varepsilon_{\mu}^{(\lambda)} T^{\mu} \quad (8)$$

with

$$T^{\mu} = \varepsilon^{\mu\nu\rho\sigma} k_{\nu} p_{\rho} q_{\sigma} A(s, t) \quad . \quad (9)$$

Here  $k$ ,  $p$  and  $q$  are the momenta of the incoming photon, the incoming nucleus and the outgoing pion, respectively.  $\varepsilon_{\nu}^{(\lambda)}$  is the polarization vector of the photon and  $A(s, t)$  is a scalar function that contains the entire dynamics of the process. This can be shown to yield:

$$\sum_{\lambda} |T^{(\lambda)}|^2 = W^2 k_{cm}^2 q_{cm}^2 \sin^2 \theta_{cm} |A(s, t)|^2 \quad . \quad (10)$$

$k_{cm}^2$  and  $q_{cm}^2$  are the three momenta of the photon and the pion,  $\theta_{cm}$  is the scattering angle and  $W$  is the total energy of the photon-nucleus system; all these quantities are taken in the cm-frame. Thus the well known  $\sin^2 \theta$ -dependence of the coherent photoproduction of pions results directly from the quantum numbers involved. The differential cross section in the cm-frame is then given by:

$$\frac{d\sigma}{d\Omega} = \left( \frac{M_A}{4\pi W} \right)^2 \frac{q_{cm}}{k_{cm}} \frac{1}{2} \sum_{\lambda} |T^{(\lambda)}|^2 \quad , \quad (11)$$

where  $M_A$  is the mass of the nucleus.

Another important consequence of Eq. (8) is, that if one replaces the photon polarization  $\varepsilon_{\mu}$  by the photon momentum  $k_{\mu}$ ,  $T^{(\lambda)}$  vanishes. Thus the amplitude  $T^{(\lambda)}$  is gauge invariant from the very beginning, independent of the model used for the nuclear ground state or the production process. This surprising result is a special feature of the coherent photoproduction which makes this reaction even more attractive from a theoretical point of view: In other reactions than the coherent one, like  $(\gamma, \pi N)$  or  $(e, e' N)$ , the usual DWIA approach leads to a gauge-dependent amplitude [22,23]. Methods to restore gauge invariance lead to considerable theoretical uncertainties [23], which do not occur in the case of coherent photoproduction.

We work in position space, since the bound state and scattering state wave functions can easily be obtained in a position space representation. In the approach described above the first diagram in Fig. 1 corresponds to the following non-local expression:

$$T_{Ndir}^{(\lambda)} = \sum_{\alpha occ.} \int d^3x d^3y \bar{\psi}_{\alpha}(\vec{x}) \phi_{\pi}^{(-)*}(\vec{x}) \Gamma_{\pi NN} G_N^o(E; \vec{x}, \vec{y}) \Gamma_{\gamma NN}^{\mu} \phi_{\mu}^{(\lambda)}(\vec{y}) \psi_{\alpha}(\vec{y}) \quad . \quad (12)$$

Here  $\psi_\alpha$  is the wave function of the bound nucleon,  $\phi_\mu^{(\lambda)}$  is the wave function of the photon, which can be assumed to be a plane wave and  $\phi_\pi^{(-)}$  is the distorted wave function of the pion satisfying incoming boundary conditions [24].  $\Gamma_{\pi NN}$  and  $\Gamma_{\gamma NN}^\mu$  are the vertices resulting from the coupling terms in Eq. (1) and  $G_N^\alpha$  is the free nucleon propagator:

$$G_N^\alpha(E; \vec{x}, \vec{y}) = \int \frac{d^3p}{(2\pi)^3} \frac{ie^{i\vec{p}(\vec{x}-\vec{y})}}{\not{p} - m} \quad . \quad (13)$$

The effect of including a dressed instead of a free nucleon propagator will be discussed in Sec. III C.

$E$  is naturally determined by energy conservation:

$$E = E_\gamma + E_\alpha \quad , \quad (14)$$

where  $E_\alpha$  is the total, relativistic energy of the bound nucleon.

To evaluate (12), we use partial-wave expansions for the wave functions as well as for the propagator [24]. Whenever derivatives appear in the vertices, we actually insert the derivatives of wave functions, so that we take into account the non-locality of the production operator. After inserting the partial-wave expansions into Eq. (12) we can perform the angular integrations analytically, since they only involve spherical harmonics. The two radial integrations are evaluated numerically.

The remaining graphs in Fig. 1 are treated analogously. For the  $\Delta$ -propagator we treat the contraction of  $\Lambda_{\mu\nu}$  from Eq. (3) with the  $\Delta N\gamma$ -vertex as one term and use the partial-wave expansion only for the remaining spin- $\frac{1}{2}$  part of the propagator:

$$\frac{\not{p} + m_\Delta}{s - m_\Delta^2 + i\sqrt{s} \Gamma(s)} \quad . \quad (15)$$

Since these expansions can only be made for a constant imaginary part of the denominator, we evaluate  $s \Gamma(s)$  at a fixed  $s_o$ , which is taken to be the invariant mass of a photon and a bound nucleon, averaged over the Fermi sphere. A further technical problem arises from the  $p_\mu p_\nu$  term in Eq. (3), since its spatial components  $p_i p_j$  contain second derivatives, an exact treatment of which would greatly complicate the calculations. We therefore approximate this term by replacing

$$p_i p_j \rightarrow k_i k_j \quad , \quad (16)$$

where  $k$  is the three-momentum of the photon. Since in momentum space the three-momentum of the  $\Delta$ -propagator is the sum of photon and nucleon momentum, this amounts to putting for this special term the three-momentum of the incoming nucleon to zero. Using this approximation, this term contributes only on the percent level, so that this assumption does not affect our results significantly.

The  $\omega NN$  form factor in Eq. (6) must also be treated separately in our approach. Since  $t = (p_\gamma - p_\pi)^2$  does not depend on the nucleon momentum, it is fixed when a plane wave is used for the pion, i.e. in PWIA. In DWIA it can be approximated using the asymptotic momentum of the pion. In the relevant kinematic region,  $t$  is small anyway as compared to

the cutoff  $\Lambda^2$ . Consequently the dependence of  $F(t)$  on the pion distortions is weak and its main effect is a renormalization of the  $\omega NN$  coupling.

The angular integrations in Eq. (12) lead to rather complicated expressions for the vertices depending on the incoming and outgoing angular momenta. The  $\sin\theta$  dependence of the differential cross section is one test for their correct numerical implementation. As a further test we have checked that for  $T^\mu$  from Eq. (9) our calculation yields:

$$T_o = 0; T_i k_i = 0 \quad , \quad (17)$$

which has to be fulfilled for each graph separately, as can be seen from the definition of this quantity.

Even though we evaluate the amplitude in position space it is instructive to consider Eq. (12) in momentum space:

$$\begin{aligned} T_{Ndir} &= \sum_{\alpha occ.} \int \frac{d^3p}{(2\pi)^3} \bar{\psi}_\alpha(\vec{p} + \vec{k} - \vec{q}) \Gamma_{\pi NN} G_N(E; \vec{p} + \vec{k}) \Gamma_{\gamma NN} \psi_\alpha(\vec{p}) \\ &= \sum_{\alpha occ.} \int \frac{d^3p}{(2\pi)^3} \bar{\psi}_\alpha(\vec{p} + \vec{k} - \vec{q}) \hat{T}_{Ndir}(E; \vec{p}, \vec{k}, \vec{q}) \psi_\alpha(\vec{p}) \quad , \end{aligned} \quad (18)$$

where for the moment we assume the pion wave function to be a plane wave. If we now make the local approximation as described above by putting the momentum of the incoming nucleon in the argument of  $\hat{T}_{Ndir}$  equal to a constant  $\vec{p}_o$ , we can rewrite Eq. (18):

$$T_{Ndir} \approx Tr \left( \hat{T}_{Ndir}(E; \vec{p}_o, \vec{k}, \vec{q}) \hat{\rho}_A(\vec{k} - \vec{q}) \right) \quad , \quad (19)$$

with the nucleonic tensor:

$$\begin{aligned} \hat{\rho}_A(\vec{p}) &= \int \frac{d^3p'}{(2\pi)^3} \sum_{\alpha occ.} \psi_\alpha(\vec{p}') \otimes \bar{\psi}_\alpha(\vec{p}' + \vec{p}) \\ &= \int d^3x e^{-i\vec{p}\vec{x}} \sum_{\alpha occ.} \psi_\alpha(\vec{x}) \otimes \bar{\psi}_\alpha(\vec{x}) \quad . \end{aligned} \quad (20)$$

One sees, that in the local approximation the differential cross section for coherent photo-production at a fixed energy involves the Fourier transformation of the nuclear ground state density, so that this cross section is proportional to a nuclear form factor. Superimposed are effects due to the non-locality of the production operator and the distortions of the pion wave function by the nucleus. Nevertheless, the differential cross section is dominated by the nuclear form factor, and the properties of the production operator itself can only be studied when the energy dependence of the cross section is considered.

#### D. The nuclear wave function

It is clear from these considerations, that it is crucial to describe the ground state properties of the nucleus realistically. The wave functions in Eq. (12) are taken from a relativistic mean-field calculation using scalar and time-like vector potentials  $V_s$  and  $V_v$ , respectively:

$$(\not{p} - m - V_v \gamma_0 - V_s) \psi_\alpha = 0 \quad . \quad (21)$$

For the potentials  $V^v$  and  $V^s$  we assume a Woods-Saxon shape:

$$V(r) = V_i^o \left( 1 + e^{\frac{(r-r_i A^{1/3})}{a_i}} \right)^{-1} \quad ; i = v, s \quad . \quad (22)$$

The parameters we use for these potentials are given in Table I. They were determined such that the separation energies [25], the root mean square radius of the charge density and the charge form factors of  $^{12}\text{C}$  and  $^{40}\text{Ca}$  [26] are well reproduced. The resulting charge form factors are shown in Figs. 3 and 4, together with the values extracted from experiment [26].

### E. The pion-nucleus interaction

It is well known, that the coherent cross section depends strongly on the interaction of the produced pion with the nucleus. This is taken into account by using a distorted pion wave function in Eq. (12), which is calculated from a position space optical potential. An optical potential as given in [27,28] is used:

$$\begin{aligned} 2E_\pi U_{opt}(r) = & -4\pi[b(r) + B(r)] \\ & + 4\pi \vec{\nabla} \{L(r)[c(r) + C(r)]\} \vec{\nabla} \\ & - 4\pi \left[ \frac{p_1 - 1}{2} \nabla^2 c(r) + \frac{p_2 - 1}{2} \nabla^2 C(r) \right] \quad , \end{aligned} \quad (23)$$

where

$$\begin{aligned} b(r) &= p_1 b_o \rho(r) \\ c(r) &= p_1^{-1} c_o \rho(r) \\ B(r) &= p_2 B_o \rho^2(r) \\ C(r) &= p_2^{-1} C_o \rho^2(r) \\ L(r) &= \left\{ 1 + \frac{4\pi}{3} \lambda [c(r) + C(r)] \right\}^{-1} \quad , \end{aligned}$$

with

$$p_1 = 1 + \frac{E_\pi}{m_N}; \quad p_2 = 1 + \frac{E_\pi}{2m_N} \quad . \quad (24)$$

$E_\pi$  is the total energy of the pion,  $m_N$  is the mass of the nucleon and  $\rho$  is the nuclear density normalized to  $A$ , obtained by summing the single particle densities in the potentials Eq. (22) over the occupied states. This optical potential contains  $s$ - and  $p$ -wave interactions of the pion via  $b(r)$  and  $c(r)$  and the so called true absorption via  $B(r)$  and  $C(r)$ . The quantity  $L(r)$  comes in because of the Lorentz-Lorenz-Ericson-Ericson effect [12]. The last term in Eq. (23) results from the so called angle transformation [12], which is a kinematical effect. The parameter  $\lambda$  is a real constant, while the quantities  $b_o$ ,  $c_o$ ,  $B_o$ , and  $C_o$  are complex and energy dependent. In [27,28] these parameters are only given for pion kinetic energies up

to 50 MeV. Since we want to compare our calculations to the A2 data, we need an optical potential for pion kinetic energies up to about 300 MeV. In order to have a consistent parameterization over this range of energies, we adopt the same form as in Eq. (23) also for higher energies. The parameters were determined by fitting the elastic scattering data of pions on  $^{12}\text{C}$  [29], including the nuclear Coulomb potential as done in [27].

Doing so one is confronted with the fact that there is a large redundancy between some of the parameters, especially between  $b_o$  and  $B_o$  and between  $c_o$  and  $C_o$  [30]. Consequently, a naive fit of all parameters leads to unphysical values. We therefore put  $B_o = 0$  and  $C_o = 0$  and determined  $b_o$  and  $c_o$  as complex, effective parameters. In Fig. 5 we show the cross sections for elastic pion scattering on  $^{12}\text{C}$  in comparison to the experimental data. In order to have one more set of parameters at higher energies, we included elastic pion scattering on  $^{16}\text{O}$  at  $T_\pi = 330$  MeV into the fitting procedure. For  $T_\pi = 100$  MeV and  $T_\pi = 157$  MeV, we were not able to find a parameter set that lead to agreement with the data beyond the second minimum of the differential cross section, without showing discrepancies at smaller angles. In these two cases we chose the optical potential parameters such that the data are reproduced well for angles up to the second minimum. In order to obtain the optical parameters as smooth functions of the pion energy, we interpolated our fit results as shown in Fig. 6.

### III. RESULTS

#### A. PWIA

The model described in the previous section was used to calculate differential and total cross sections for the coherent photoproduction of pions on nuclei. In Fig. 7 and Fig. 8 we show our results for plane wave impulse approximation (PWIA), i.e. with a free outgoing pion. As has been discussed at the end of Sec. II C, the total cross section shows the resonant character of the elementary production operator, while the shape of the differential cross section results from the nuclear form factor (multiplied with  $\sin^2 \theta$ ). In Fig. 7 we also show the contributions of the different diagrams. Clearly, the  $\Delta$ -resonance dominates the process, but the other diagrams lead to sizable corrections that should not be neglected. The omega contribution comes only from the vector coupling of the omega (Eq. (1)), the tensor coupling contributes only negligibly.

It is now instructive to consider the non-relativistic and the local approximation, which have been used in previous studies [8–11]. To do so, we also made calculations employing for the direct  $\Delta$ -part the non-relativistic production operator from [8]. There the exchange graph of the  $\Delta$ -is neglected and the  $\Delta$ -width is assumed to be constant. In our model, using this non-relativistic operator corresponds to neglecting the lower components of the nuclear wave functions and of the  $\Delta$ -propagator. The result is shown in Fig. 9. Since the non-relativistic curve in this figure only contains contributions from the upper components of the relativistic bound state wave functions, it is not completely equivalent to the non-relativistic calculation in [9], where non-relativistic wave functions are used. Nevertheless, we can conclude about the relative size of relativistic effects, which can in this case be as large as 30%.

The local approximation was implemented by putting the momentum of the incoming nucleon in the argument of the production operator equal to zero, i.e. the nucleon is assumed to be initially at rest. The result is also shown in Fig. 9. The difference between the two non-relativistic versions of our model can be understood from Eq. (18) for the direct  $\Delta$ -diagram: If the dependence of the production operator on the incoming nucleon momentum  $\vec{p}$ , is taken into account, the  $\Delta$ -peak is smeared out because of the integration over  $\vec{p}$ . Thus the non-local calculation shows in comparison to the local result a lower, broader  $\Delta$ -peak, which is also shifted to higher energies.

## B. DWIA

We now take the final state interaction of the pion with the nucleus into account by means of the optical potential given in Eq. (23). The resulting total and differential cross sections for  $^{12}\text{C}$  and  $^{40}\text{Ca}$  are shown in Figs. 10, 11 and 12 in comparison to PWIA results. For the case of  $^{40}\text{Ca}$  we took the same parameters for the pion optical potential as for  $^{12}\text{C}$ . For  $E_\gamma \lesssim 230$  MeV, i.e. for  $T_\pi \lesssim 100$  MeV, where the absorption is relatively small (cf. Fig. 6), the distortion of the pion wave function leads to an increase of the total cross section, indicating the importance of off-shell effects in the pion distorted wave. For higher photon energies the cross section is strongly reduced because of the large imaginary part of the pion optical potential. This reduction is stronger in the case of  $^{40}\text{Ca}$ , since the absorption of pions increases with the nuclear mass. Besides that, the curves for the two different nuclei are very similar in shape, and differ mainly by a global factor. Making an ansatz  $\sigma \sim A^\alpha$  we find  $\alpha \sim 0.7$  for the case of PWIA. This rather weak A-dependence results from the different momentum dependence of the nuclear form factor for  $^{12}\text{C}$  and  $^{40}\text{Ca}$  (cf. Figs. 3 and 4): For a given momentum transfer, the  $^{40}\text{Ca}$  form factor is much smaller than the one for  $^{12}\text{C}$ , which compensates for the fact that there are  $A$  amplitudes to be summed for a given nucleus (Eq. (12)). For the DWIA results we find the smaller value  $\alpha \sim 0.5$ - $0.6$ , depending on the photon energy. This somewhat smaller value again reflects the stronger pion absorption on  $^{40}\text{Ca}$ .

At this point it must be kept in mind, that two different but phase-equivalent optical potentials might yield the same elastic scattering cross section, but lead to a different behavior of the pion wave function in the nuclear interior. Since in Eq. (12) the pion wave function within the nucleus, rather than its asymptotic behavior, is relevant, two phase equivalent optical potentials might in principle lead to different results for the coherent photoproduction of pions.

In order to explore this possible ambiguity, we have also performed calculations with the parameter sets given in [27] and [28] for  $T_\pi = 50$  MeV ( $E_\gamma = 184$  MeV). Using these parameter sets, in which the parameters  $B_o$  and  $C_o$  are non-zero, we get a total cross section that differs from the one obtained with our pion optical potential by less than 10 % at this specific pion energy. This indicates that our results depend only weakly on the concrete version of the optical potential. At higher energies the 50 MeV parameters from [27,28] and our energy dependent optical potential lead to cross sections that differ strongly, which shows the importance of including properly the energy dependence of the parameters shown in Fig. 6.

In Fig. 13 results for a DWIA as well as for a PWIA calculations are shown in comparison to the A2 data [4]. While the PWIA yields a completely wrong shape, the DWIA reproduces the energy dependence of the data well, but overshoots the data on the maximum by about 15 %.

As mentioned above, the  $\omega NN$  vector coupling constant and the form factor (Eq. (6)), which lead to the  $\omega$  contribution in Fig. 7, are not accurately known. In the elementary photoproduction of neutral pions the contribution of the omega graph to the differential cross section is about 10 %, depending on the angle. To show the dependence of our result for the coherent photoproduction on the omega parameters, we show in Fig. 14 calculations employing different values of  $g_{\omega NN}^v$  and  $\Lambda$ . One sees from Fig. 14 that the height of the maximum in the data could be reproduced better with a different choice of values for the omega coupling and the cutoff. The value of  $g_{\omega NN}^v=8$ , however, which is used to obtain the lower curve in Fig. 14, results from  $SU(3)$  considerations, which predict  $g_{\omega NN} = 3g_{\rho NN}$ . The values for these couplings extracted from  $NN$ -scattering do not fulfill this relation [16]. We therefore use  $g_{\omega NN}=10$ , which has been determined from  $NN$ -scattering [13].

### C. Medium effects

So far we have used the same production operator as in vacuum. Since it contains propagators of strongly interacting particles, the possibility of medium modifications of the production operator through modifications of the intermediate propagators has to be taken into consideration.

For the nucleon propagator we include medium effects by replacing the free propagator with the one obtained from the mean-field in which the bound state wave functions were calculated. We thus employ a dressed nucleon propagator  $G_N$  that fulfills

$$(\not{p} - m - V_v \gamma_0 - V_s)G_N(p_0; \vec{x}, \vec{y}) = i\delta^3(\vec{x} - \vec{y}) \quad . \quad (25)$$

Since  $G_N$  is calculated in the mean-field approximation, it contains the static properties of a struck nucleon interacting with the residual nucleus. It is the natural extension of the elementary model to reactions on the nucleus, in which the bound and the intermediate nucleon are treated consistently. In Fig. 15 we show results of calculations for  $^{12}C$  using the free as well as the dressed nucleon propagator from Eq. (25). The decrease of the cross section results from the fact, that the total contribution of the nucleon terms is the result of an approximate cancellation of direct and exchange graph; in the case of the dressed nucleon propagator, this cancellation is more complete, leading to a smaller net contribution.

For the  $\Delta$ -resonance it is well known, that it feels an attractive potential of about -30 MeV at normal nuclear density [12], which might have an effect on any production process involving the  $\Delta$ . Indeed, in  $(^3He, t)$  and  $(d, ^2He)$  reactions a shift of the  $\Delta$ -peak relative to the reaction on the proton has been observed [31,32]. A considerable part of this shift is, however, due to trivial effects e.g. the energy dependence of the nuclear form factor, so that it is only partially a consequence of in-medium modifications of the  $\Delta$  [33,34]. In contrast to that, the  $\Delta$ -peak remains essentially unshifted in the photoabsorption on nuclei [35].

Calculating the full, relativistic  $\Delta$ -propagator in the presence of nuclear potentials is out of the scope of this work. We effectively take the attraction of a  $\Delta$ -within a nucleus

into account by shifting its mass in the production operator. In Fig. 15 we show results of a calculation with the  $\Delta$ -mass reduced by 15 MeV. While the dressed nucleon propagator leads to a decrease of the cross section for all energies, a mass shift of the  $\Delta$  increases the cross section at lower energies and decreases it at higher energies. The value  $\delta m_\Delta = -15$  MeV has been chosen since for this value the absolute height of the maximum of the A2 data is reproduced (Fig. 16). Since this number can only be interpreted as an average over the entire nucleus, it seems to be quite reasonable in comparison to the depth of the  $\Delta$ -potential of 30 MeV [12]. It must at this point be kept in mind, that the actual value of  $\delta m_\Delta$ , determined by comparison to the data, depends to some extent on the value used for the  $\omega NN$  coupling constant.

Besides the mass, the width of the  $\Delta$  might also be modified in the medium. However, in this case the situation is less clear: A simple analysis taking into account Pauli blocking and collisional broadening leads to a width that is rather independent of the nuclear density [36]. In contrast to that, delta-hole calculations predict an increase of the width by as much as 60 MeV [37]. In Fig. 16 we also show the results of a calculation employing a  $\Delta$ -width that is increased by 30 MeV, which leads to visible effects only at higher energies. Thus for the A2 data we can clearly distinguish between the effect of a modified mass and a modified width of the  $\Delta$ .

As can be seen in Fig. 16, the inclusion of a dressed nucleon propagator and a lowered  $\Delta$ -mass clearly improves the agreement with the data around the maximum. At higher energies, the situation is not clear. The in-medium production operator seems to lead to an underestimation of the data for  $E_\gamma > 350$  MeV. More experimental data, especially at smaller angles, are needed in this energy range before definite conclusions can be drawn.

Since there is no reliable information available on the modification of an omega meson with space-like momentum in nuclear matter, we did not consider an in-medium modification of the corresponding graph.

The special energy dependence of the differential cross section at a constant angle is the result of an interplay between the energy dependence of the production operator and the nuclear form factor. In order to circumvent the energy dependence of the form factor, as well as to eliminate the trivial  $\sin^2\theta$  term (Eq. (10)), we show in Fig. 17 the differential cross section for a constant momentum transfer  $|\vec{q}| = 0.1$  GeV, divided by  $\sin^2\theta$  as a function of the photon energy for  $^{12}\text{C}$  and  $^{40}\text{Ca}$ . When plotting the cross section this way, the in-medium modifications of the production operator lead to a strong effect, visible over a large range of energies. Especially an increased  $\Delta$ -width now leads to a pronounced effect. Thus the new TAPS data, that will cover a large range of angles for each energy [38], might allow to distinguish between the different cases in Fig. 17.

#### IV. SUMMARY AND CONCLUSIONS

We have presented a relativistic and non-local model for the coherent photoproduction of pions on nuclei. Since the calculation for this process is gauge invariant, and since only a minimum amount of theoretical input is needed, this reaction represents an attractive field to test our understandings of hadrons and nuclei.

The production operator employed was derived from an effective Lagrangian for which the

free parameters were fixed by comparison to the data for elementary processes. Applying this production operator to the photoproduction on a nucleus involves an off-shell extrapolation with respect to the nucleon. In our model we used the off-shell behavior following naturally from an effective field theory. The validity of this extrapolation, as well as the DWIA assumption that only one nucleon is involved in the production process, can only be tested in comparison to experimental data.

We have shown, that non-relativistic as well as local approximations can lead to considerable uncertainties. Our results depend somewhat on the value used for the  $\omega NN$  coupling constant, which is not well known. However, the resulting uncertainties are less than 10 %. Employing the same production operator as in vacuum leads to a good reproduction of the shape of the A2 data, but a slight overestimation of the absolute value. The agreement with these data could be improved by taking into account medium modifications of the production operator via modifications of the nucleon and  $\Delta$ -propagators.

We conclude that the relativistic DWIA, employing a realistic production operator is an adequate approach to the coherent photoproduction of pions on nuclei. More experimental data on this process will present a further test of our model and might allow more conclusions about the role of medium effects.

#### ACKNOWLEDGMENTS

We would like to thank the A2-collaboration at MAMI for providing us with their data prior to publication. We gratefully acknowledge many helpful discussions with R. Shyam in an early stage of this work. We also would like to thank Thomas Feuster for performing the elementary calculations.

## REFERENCES

- [1] Th. Feuster et al., *Nucl. Phys.* **A612**, (1997) 375.
- [2] J. Arends et al., *Z. Phys.* **A311**, (1983) 367.
- [3] R. W. Gothe et al., *Phys. Lett.* **B355**, (1995) 59.
- [4] M. Schmitz, Dissertation, Johannes Gutenberg-Universität Mainz, Mainz 1996, to be published.
- [5] R.C. Carrasco et al., *Nucl. Phys.* **A565**, (1993) 797.
- [6] B. Körfgen et al., *Phys. Rev.* **C50**, (1994) 1637.
- [7] E. Oset et al., *Nucl. Phys.* **A368**, (1981) 375; *Nucl. Phys.* **A402**, (1983) 612;.
- [8] S. Boffi et al., *Nuovo Cim.* **A104**, (1991) 843.
- [9] S. Boffi et al., *Nucl. Phys.* **A448**, (1986) 637.
- [10] A.A. Chumbalov et al., *Z. Phys.* **A328**, (1987) 195.
- [11] A.A. Chumbalov et al., *Phys. Lett.* **B196**, (1987) 23.
- [12] T. Ericson und W. Weise, *Pions and Nuclei*, Calderon Press, Oxford, 1988
- [13] W. Grein et al., *Nucl. Phys.* **A338**, (1980) 332.
- [14] M. Benmerrouche et al., *Phys. Rev.* **D51**, (1995) 3237.
- [15] R.M. Davidson et al., *Phys. Rev.* **D43**, (1991) 71.
- [16] O. Dumbrajs et al., *Nucl. Phys.* **B216**, (1993) 277.
- [17] H. Garcilazo et al., *Nucl. Phys.* **A562**, (1993) 521.
- [18] I. Blomquist et al., *Nucl. Phys.* **A280**, (1977) 405.
- [19] D. Menze et al., ZAED Compilation of Pion Photoproduction Data, University of Bonn, 1977.  
Landolt-Börnstein *Total Cross Sections for Reactions of High-Energy Particles*, Vol. I/12b, Berlin, 1988.
- [20] X. Li et al., *Phys. Rev.* **C48**, (1993) 816.
- [21] J. Piekarewicz et al., *Phys. Rev.* **C55**, (1997) 2571.
- [22] J.I. Johansson et al., *Nucl. Phys.* **A575**, (1994) 477.
- [23] S. Pollock et al., *Phys. Rev.* **C53**, (1996) 2304.
- [24] C. J. Joachain, *Quantum collision theory*, 3rd edition, North Holland Physics Publishing, Amsterdam 1983.
- [25] G. Audi et al., *Nucl. Phys.* **A595**, (1995) 409.
- [26] H. de Vries et al., *At. Data Nucl Data Tables* **36** (1987) 495.
- [27] K. Stricker et al., *Phys. Rev.* **C22**, (1980) 2043.
- [28] J. A. Carr et al., *Phys. Rev.* **C25**, (1982) 952.
- [29] Preedom et al., *Phys. Rev.* **C23**, (1981) 1134;  
Blecher et al., *Phys. Rev.* **C20**, (1979) 1884;  
Leitch et al., *Phys. Rev.* **C29**, (1984) 561;  
Antonuk et al., *Nucl. Phys.* **A420**, (1984) 435;  
Piffaretti et al., *Phys. Lett.* **B71**, (1977) 324;  
Albanese et al., *Nucl. Phys.* **A350**, (1980) 301.
- [30] T. Seki et al., *Phys. Rev.* **C27**, (1983) 2799.
- [31] C. Ellegaard et al., *Phys. Rev. Lett.* **59**, (1987) 974.
- [32] D. Contardo et al., *Phys. Lett.* **B168**, (1986) 331.
- [33] J. Delorme et al., *Phys. Lett.* **B263**, (1991) 157.

- [34] T. Udegawa et al., *Phys. Lett.* **B245**, (1990) 1.
- [35] N. Bianchi et al., *Phys. Lett.* **B325**, (1994) 333.
- [36] M. Effenberger et al., *Nucl. Phys.* **A613**, (1997) 353.
- [37] E. Oset et al., *Nucl. Phys.* **A468**, (1987) 631.
- [38] B. Krusche, private communication.

TABLES

Nucleus	$V_v$ (MeV)	$r_v$ (fm)	$a_v$ (fm)	$V_s$ (MeV)	$r_s$ (fm)	$a_s$ (fm)
$^{12}C$	385.7	1.056	0.427	-470.4	1.056	0.447
$^{40}Ca$	348.1	1.149	0.476	-424.5	1.149	0.506

TABLE I. Potential parameters for the bound states.

FIGURES

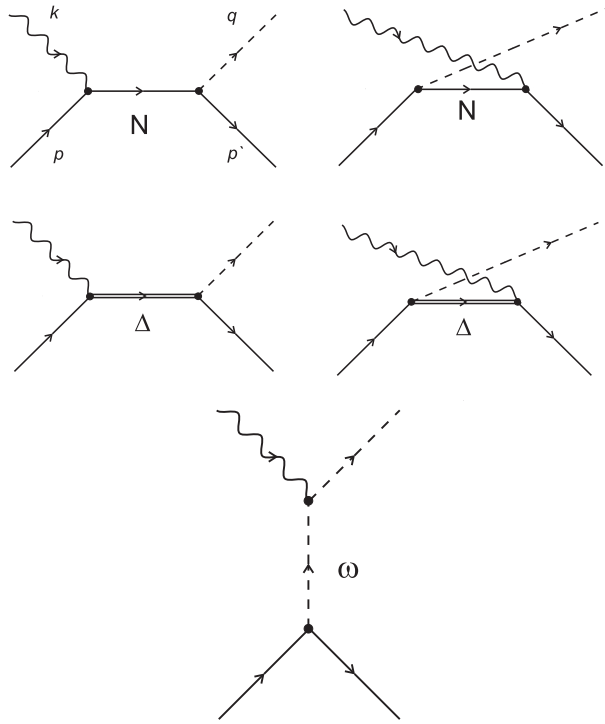


FIG. 1. Feynman diagrams contributing the photoproduction of neutral pions.

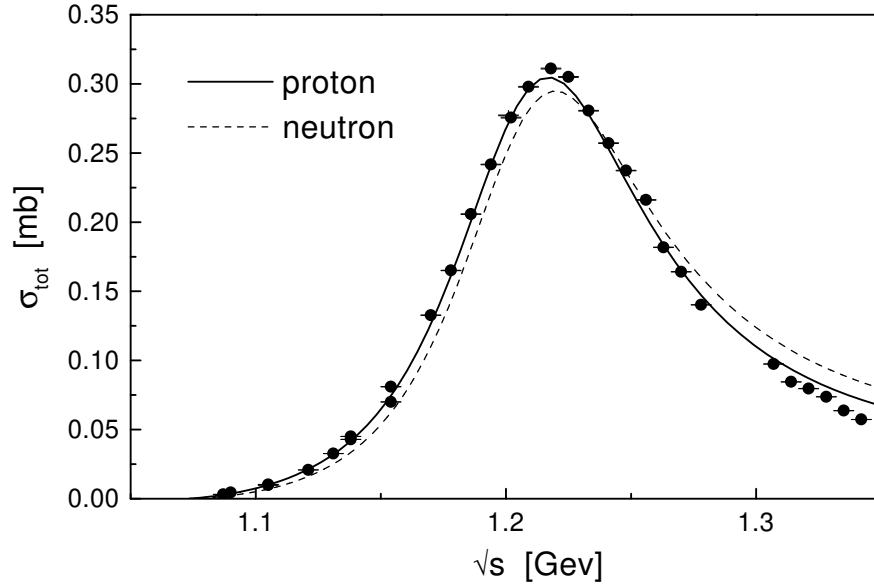


FIG. 2. Total cross section for the photoproduction of neutral pions on a single nucleon. The curves give the results of calculations employing the Lagrangian given in Eq. (1). The data are for the reaction  $\gamma p \rightarrow p\pi^0$  and are taken from [19].

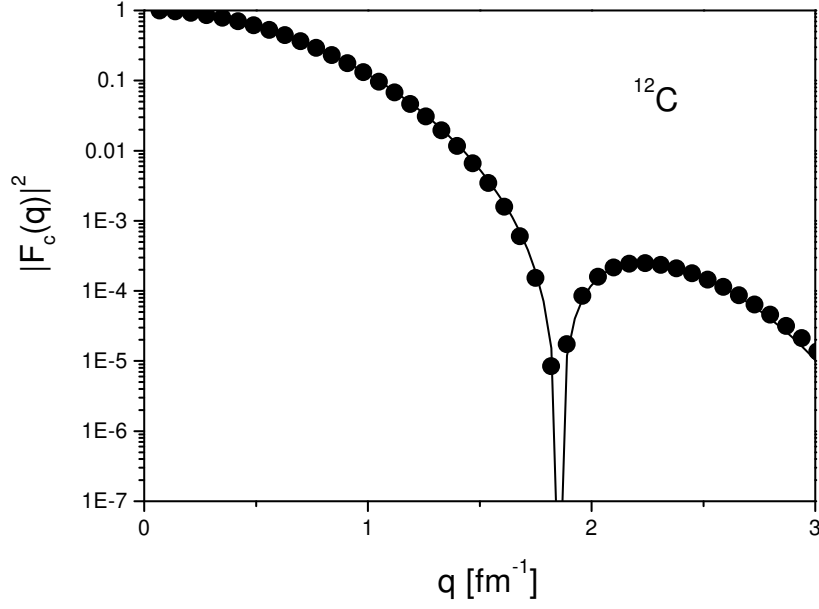


FIG. 3. Charge form factor for  $^{12}\text{C}$  resulting from the wave functions used in this work in comparison to values extracted from experiment [26].

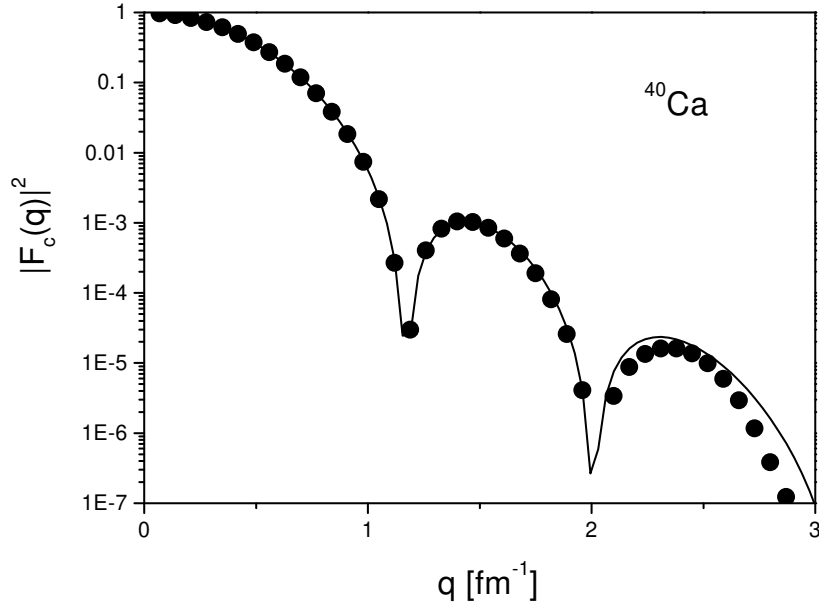


FIG. 4. Same as Fig. 3, but for  $^{40}\text{Ca}$ .

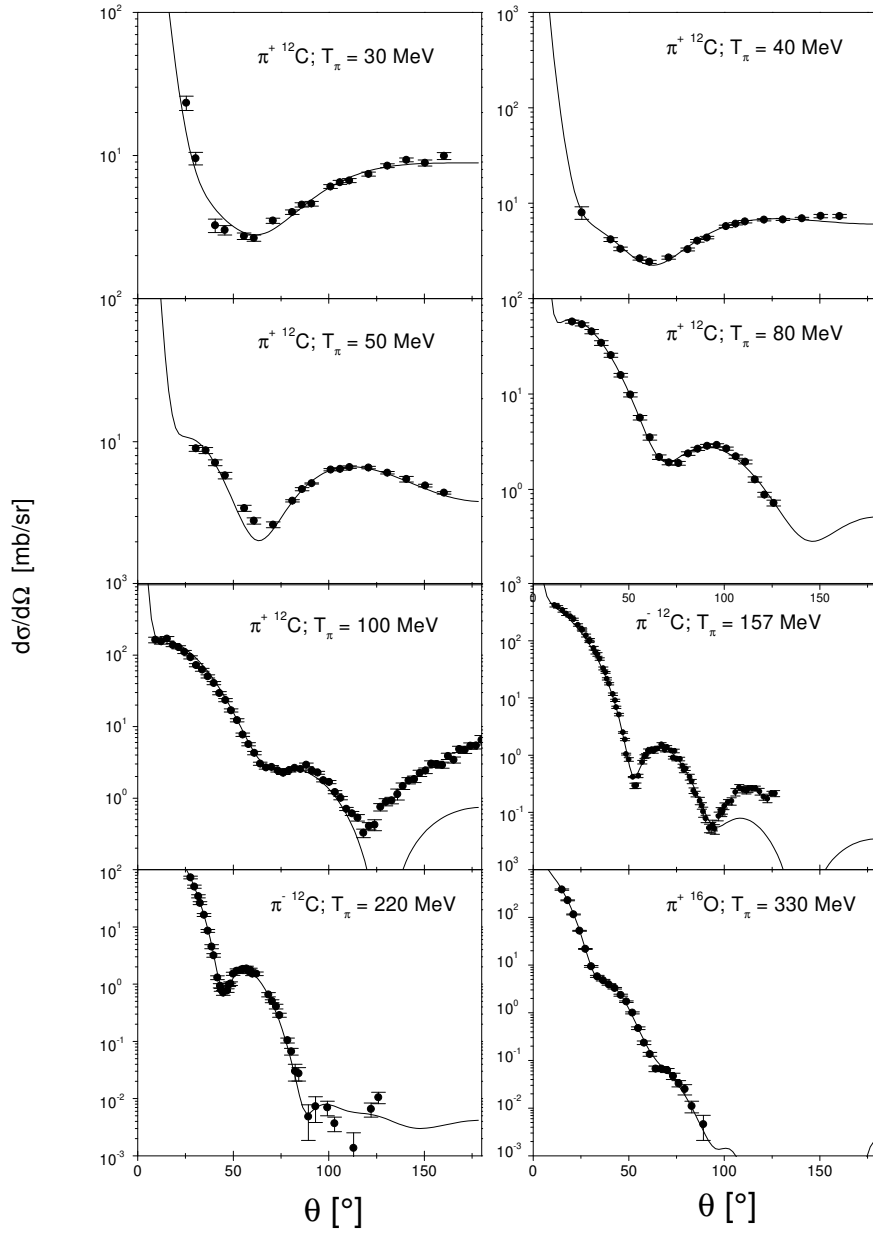


FIG. 5. Fit results for elastic pion scattering as described in the text. the data are taken from Ref. [29].

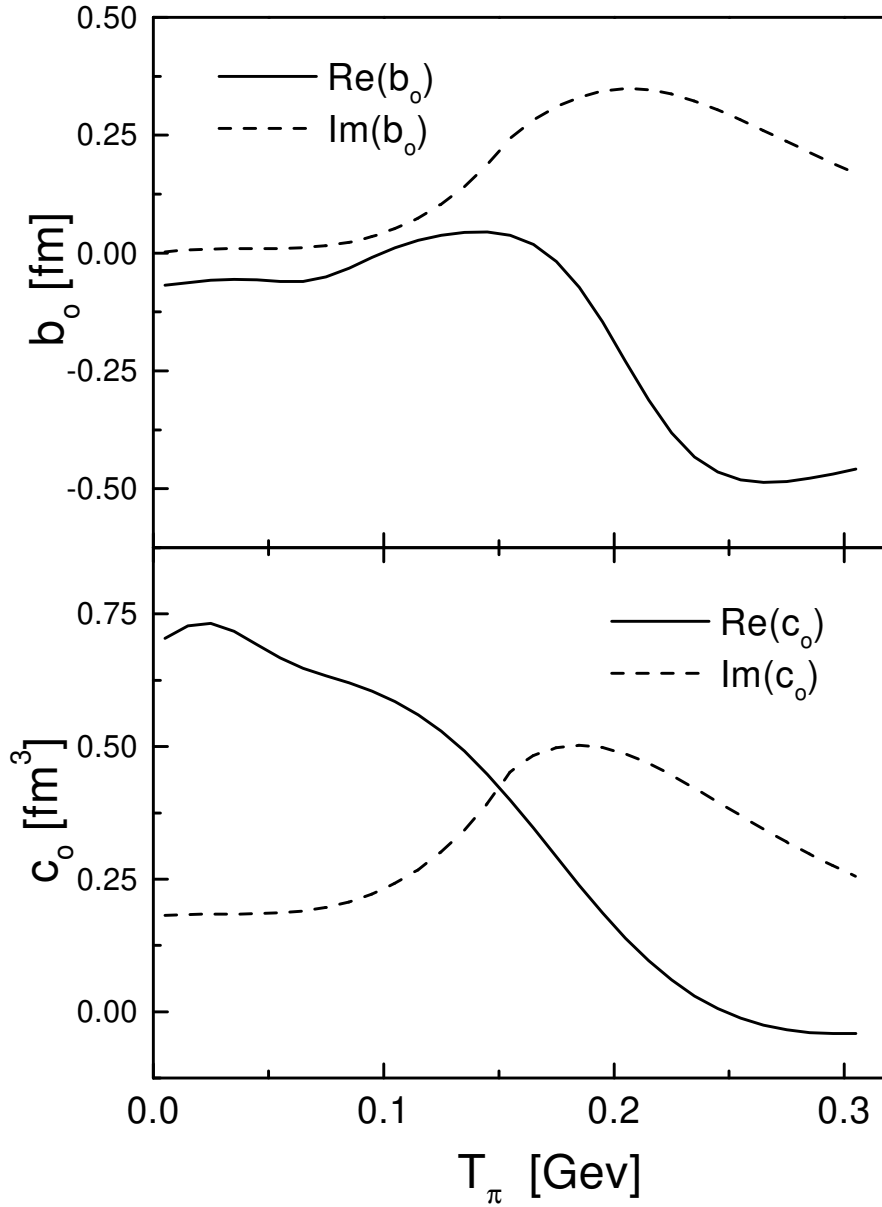


FIG. 6. Energy dependence of the  $s$ - and  $p$ -wave parameters for the pionic optical potential resulting from our fit as described in the text.

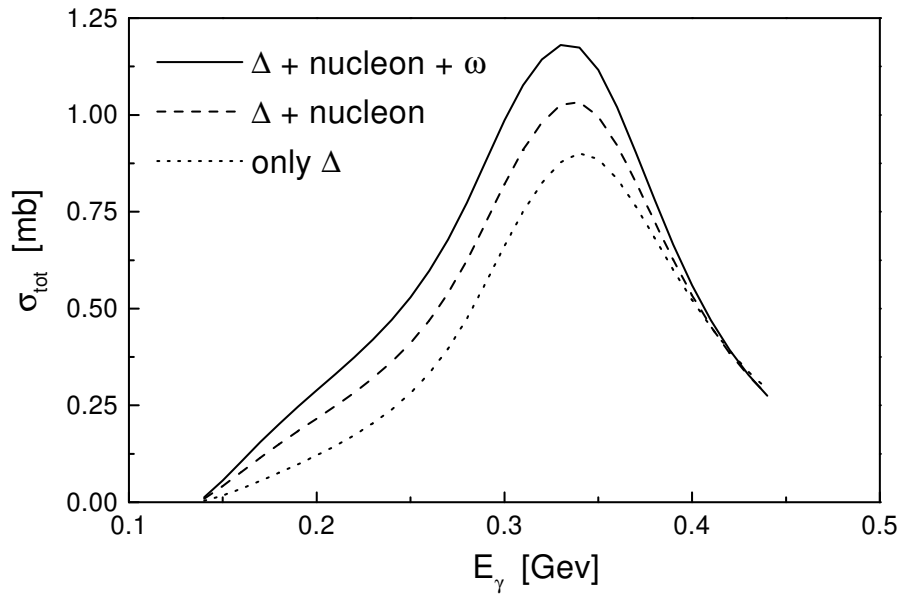


FIG. 7. Total cross section for  $^{12}\text{C}(\gamma, \pi^0)^{12}\text{C}$  in PWIA.

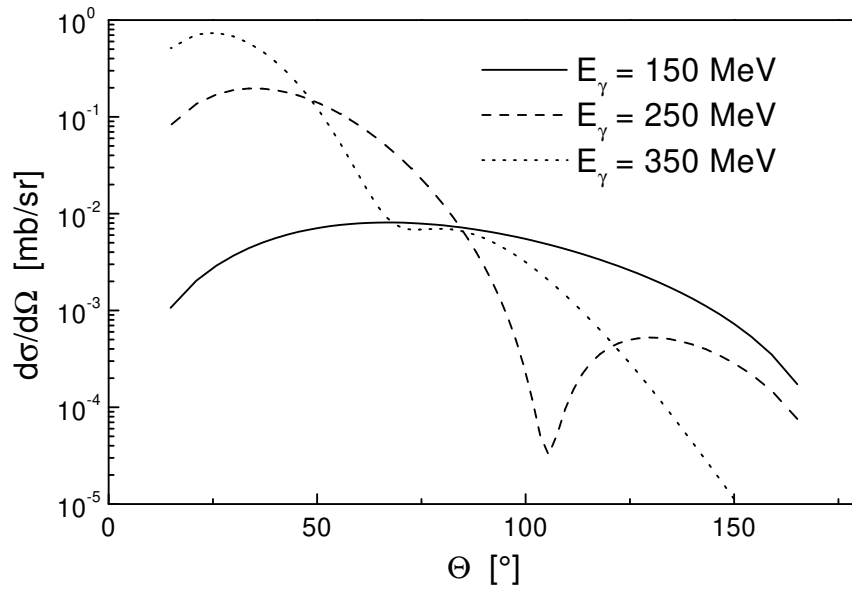


FIG. 8. Differential cross section for  $^{12}\text{C}(\gamma, \pi^0)^{12}\text{C}$  in PWIA for three different energies.

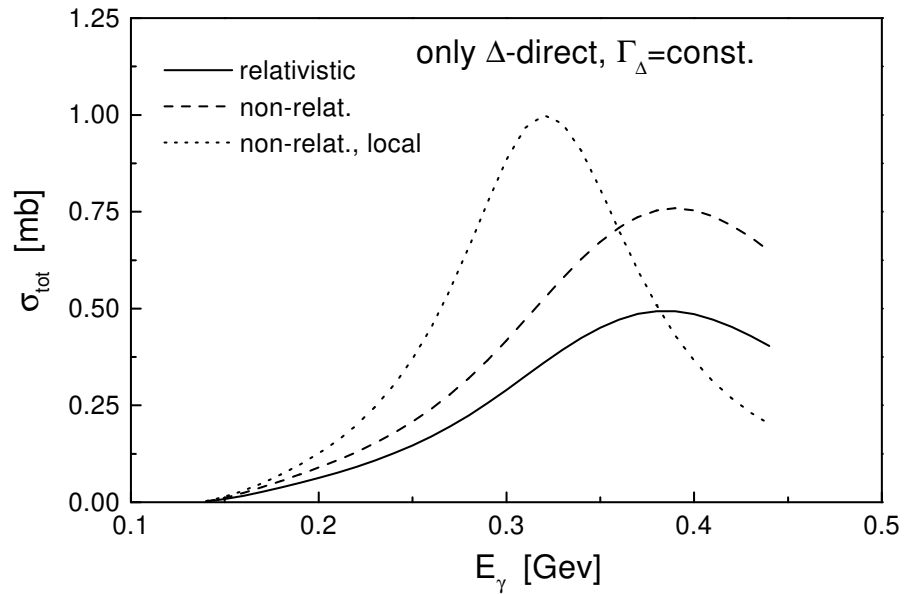


FIG. 9. Effects of different approximations: The direct  $\Delta$ -graph with a constant width is evaluated exactly, in a non-relativistic and a local approximation as described in the text.

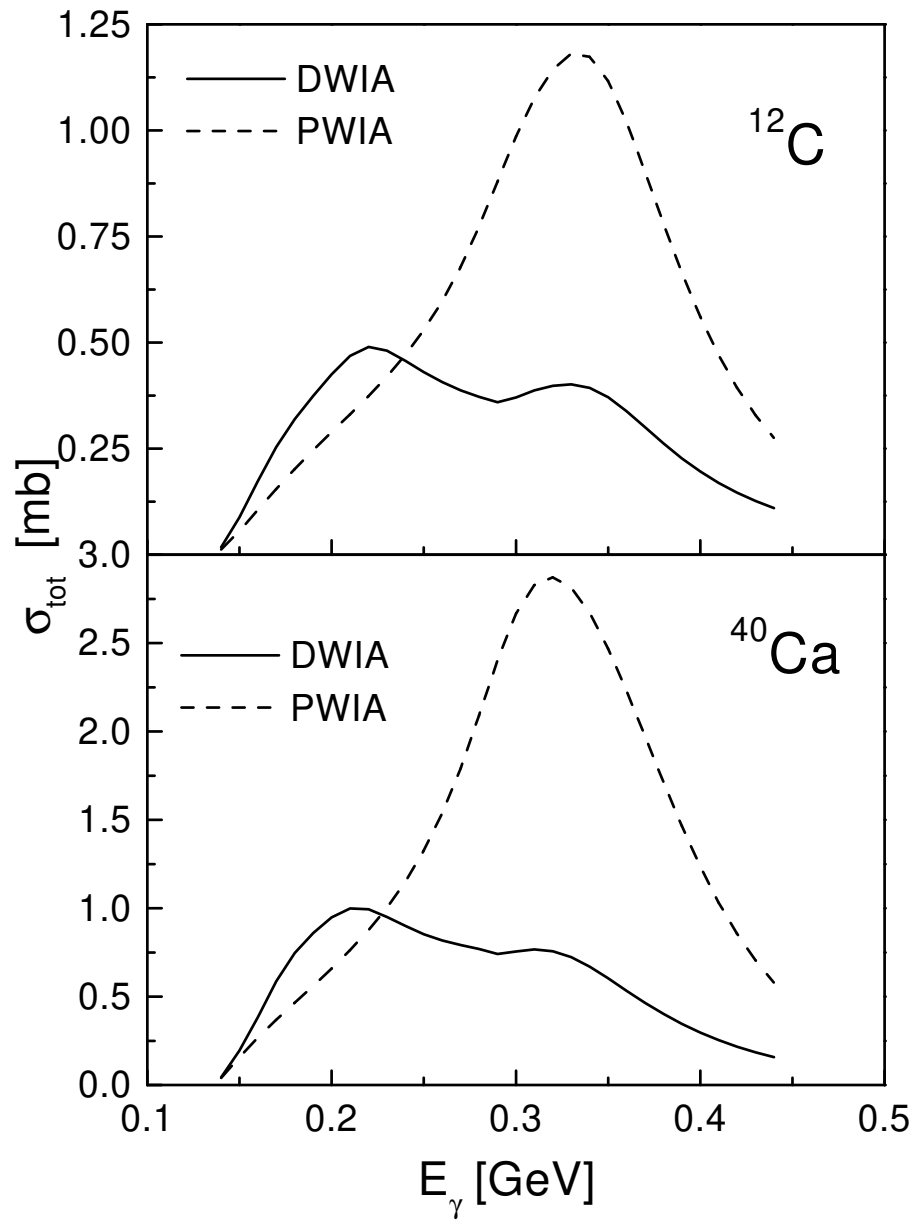


FIG. 10. Total cross section in DWIA and PWIA for  $^{12}\text{C}(\gamma, \pi^0)^{12}\text{C}$  and  $^{40}\text{Ca}(\gamma, \pi^0)^{40}\text{Ca}$ .

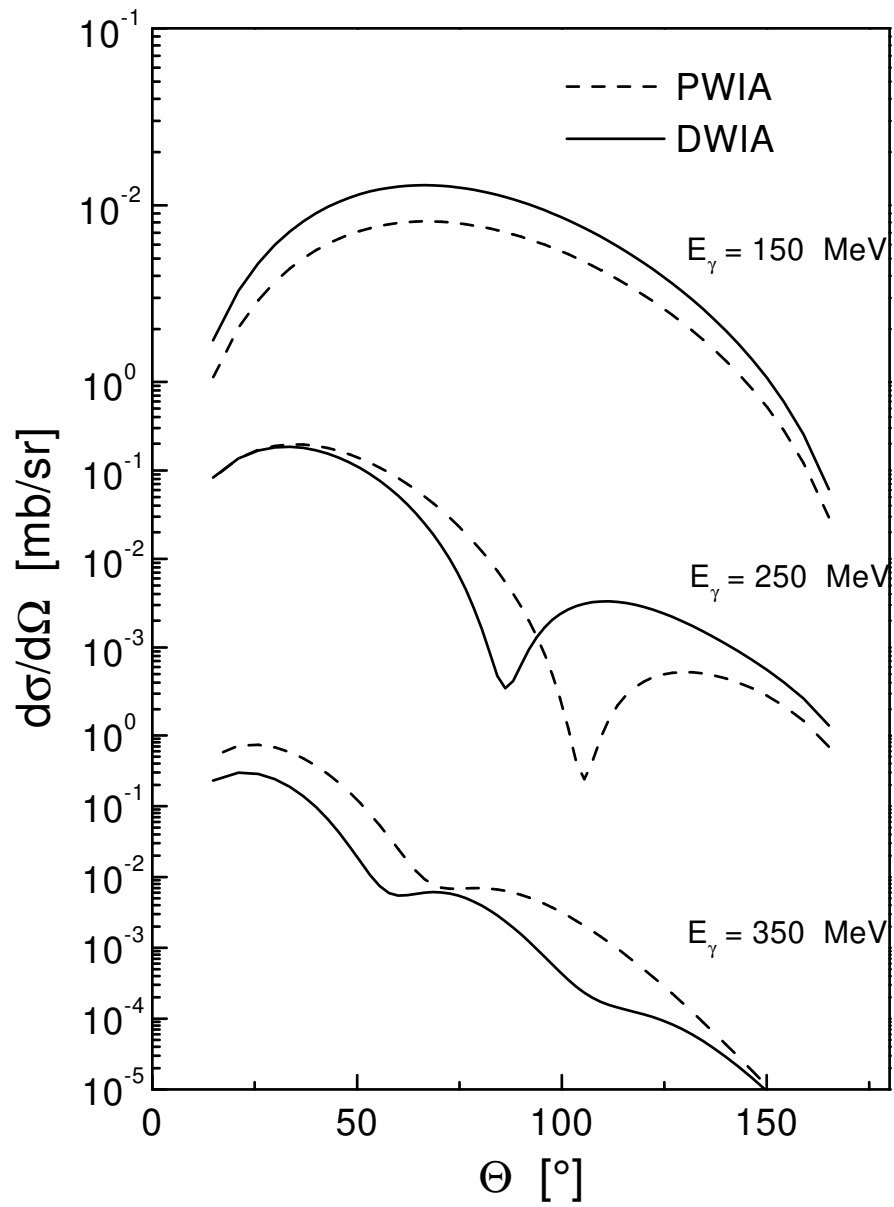


FIG. 11. Differential cross section in DWIA and PWIA for  $^{12}\text{C}(\gamma, \pi^0)^{12}\text{C}$ .

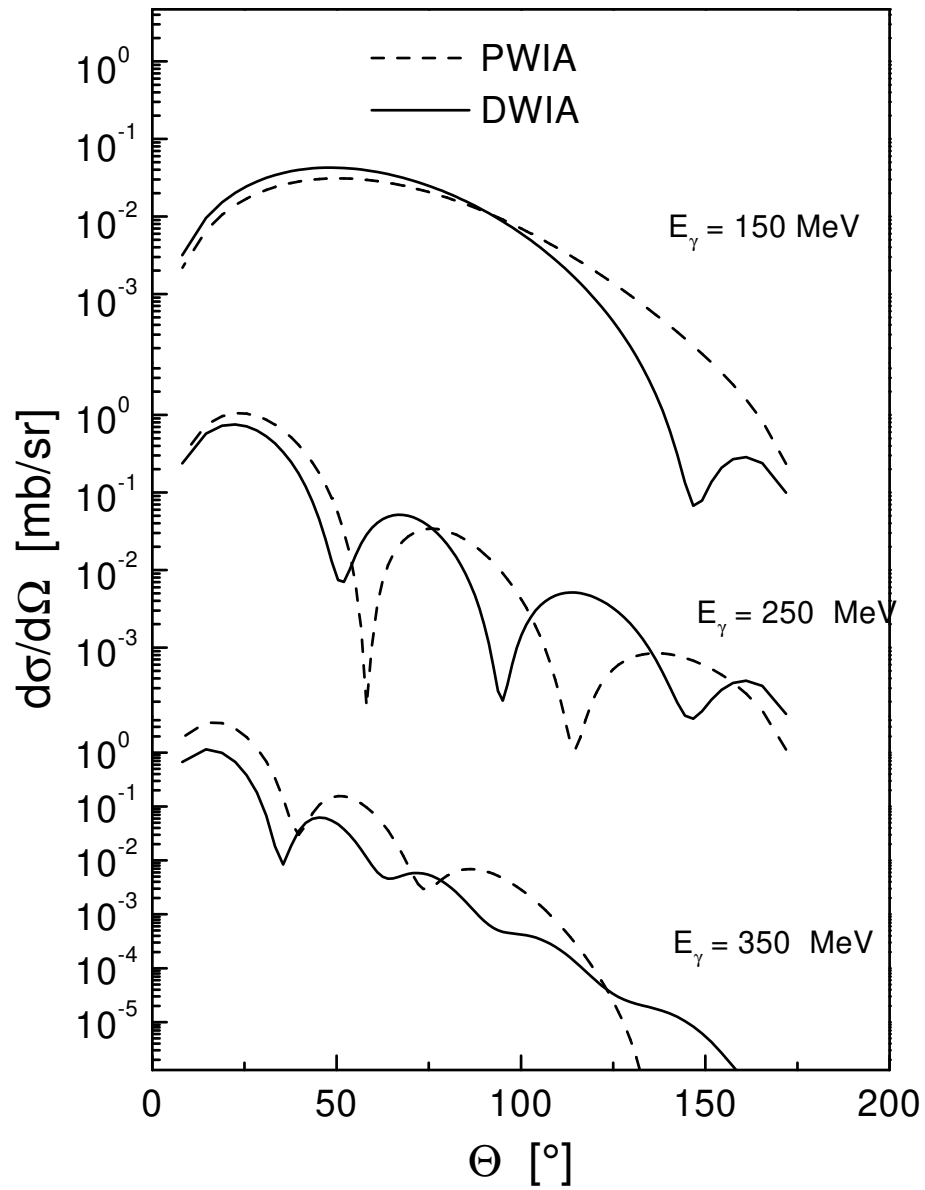


FIG. 12. Differential cross section in DWIA and PWIA for  $^{40}\text{Ca}(\gamma, \pi^0)^{40}\text{Ca}$ .

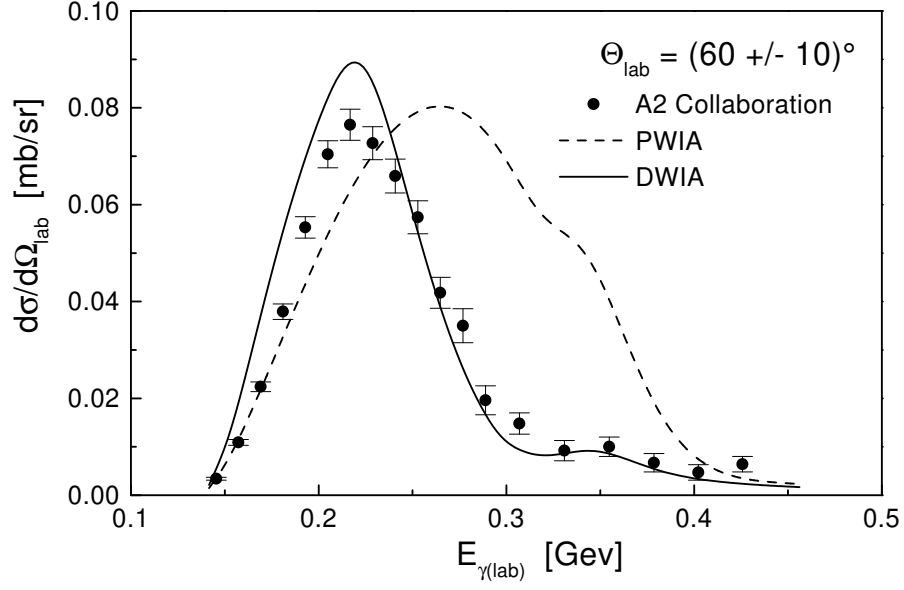


FIG. 13. Comparison of the A2-data for  $^{12}\text{C}$  to a DWIA and a PWIA calculation.

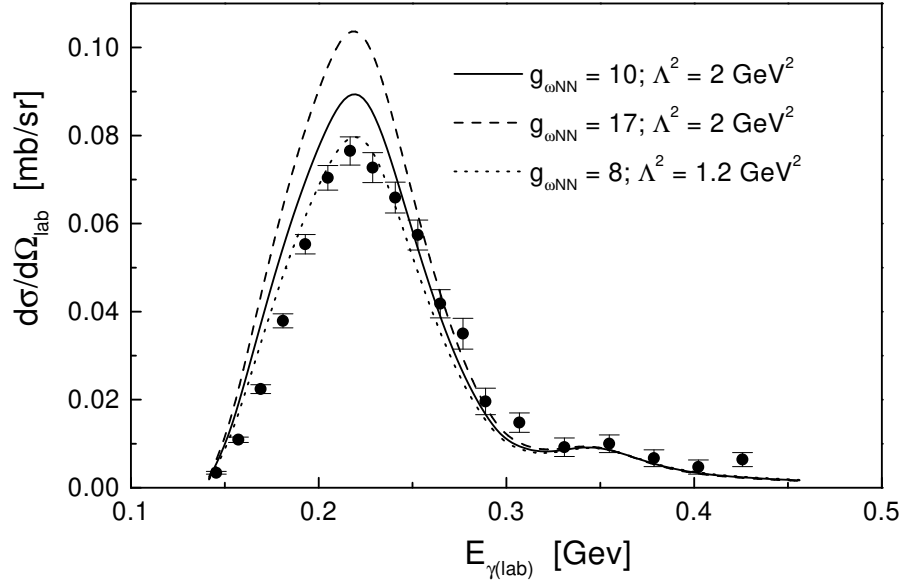


FIG. 14. Same as Fig. 13, but for different  $\omega NN$  couplings.

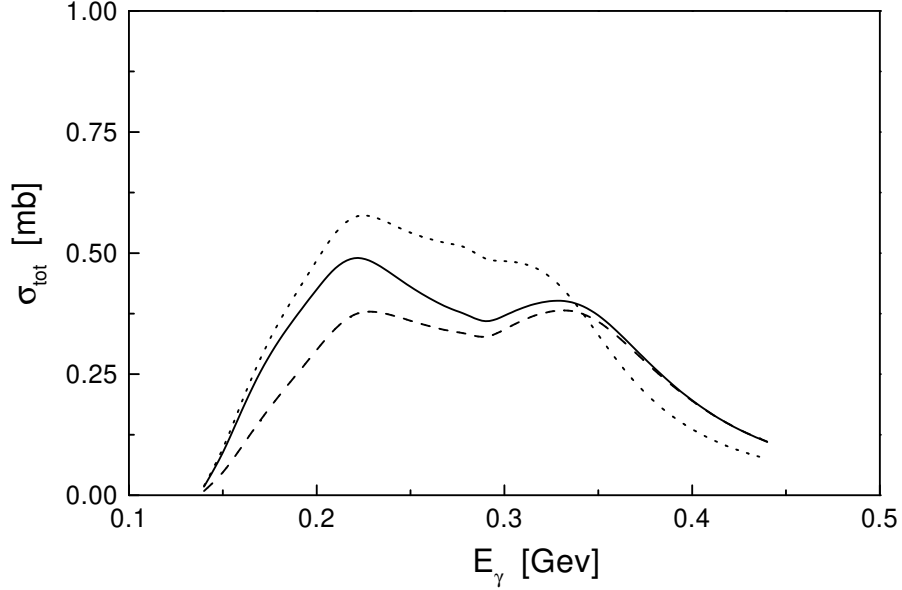


FIG. 15. Total DWIA cross section for  $^{12}\text{C}(\gamma, \pi^0)^{12}\text{C}$  using the free production operator (full line), using the dressed nucleon propagator (dashed line) as described in the text, and with a mass shift of the  $\Delta$   $\delta m_\Delta = -15$  MeV (dotted line).

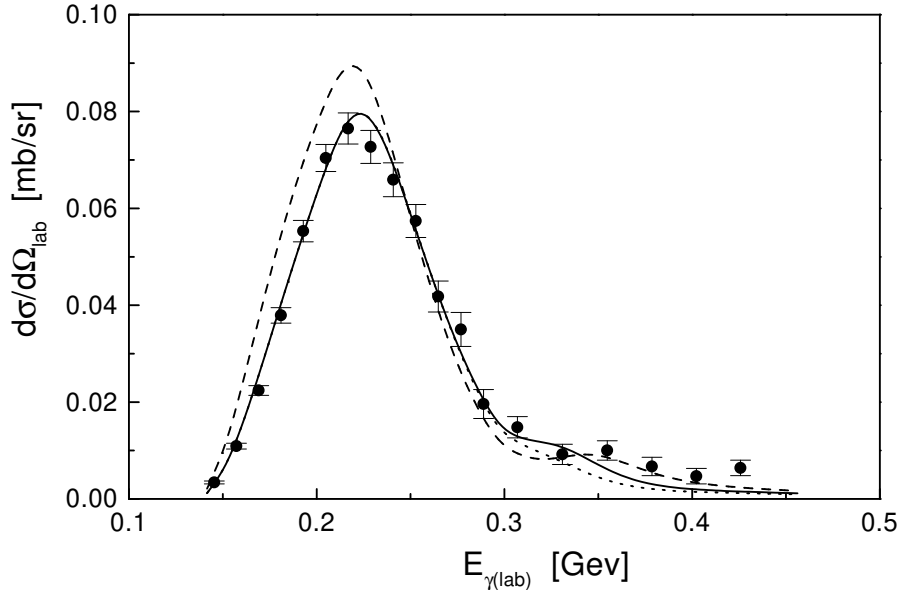


FIG. 16. Same as Fig. 13, but with a free production operator (dashed line), an in-medium production operator with a dressed nucleon propagator and a  $\Delta$ -mass shift  $\delta m_\Delta = -15$  MeV (full line), and with an in-medium production operator including additionally an increased  $\Delta$ -width  $\delta \Gamma_\Delta = 30$  MeV (dotted line).

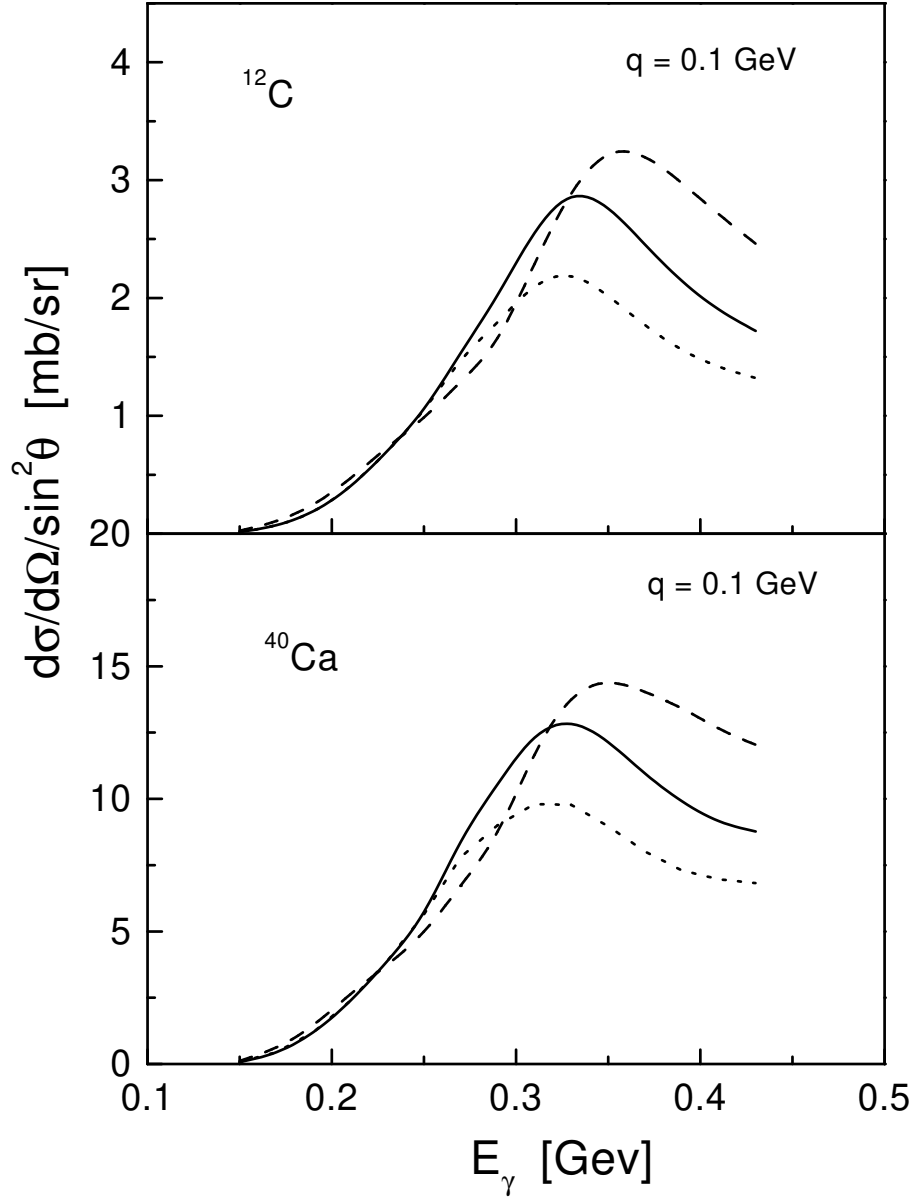


FIG. 17. Differential cross section divided by  $\sin^2 \theta$  for  $^{12}\text{C}(\gamma, \pi^0)^{12}\text{C}$  and  $^{40}\text{Ca}(\gamma, \pi^0)^{40}\text{Ca}$  for a fixed momentum transfer of 0.1 GeV. The labeling of the curves is the same as in Fig. 16: free production operator (dashed line), in-medium production operator with a dressed nucleon propagator and a  $\Delta$ -mass shift  $\delta m_\Delta = -15$  MeV (full line), and with an in-medium production operator including additionally an increased  $\Delta$ -width  $\delta \Gamma_\Delta = 30$  MeV (dotted line).